THE JOURNAL OF PHYSICAL CHEMISTRY B
A JOURNAL OF THE AMERICAN CHEMICAL SOCIETY

pubs.acs.org/JPCB

Article

Plant Terpenoid Permeability through Biological Membranes Explored via Molecular Simulations

Published as part of The Journal of Physical Chemistry virtual special issue "Early-Career and Emerging Researchers in Physical Chemistry Volume 2".

Saad Raza, Mykayla Miller, Björn Hamberger, and Josh V. Vermaas*

Cite This: *J. Phys. Chem. B* 2023, 127, 1144–1157

Read Online

ACCESS | Metrics & More | Article Recommendations | Supporting Information

ABSTRACT: Plants synthesize small molecule diterpenes composed of 20 carbons from precursor isopentenyl diphosphate and dimethylallyl disphosphate, manufacturing diverse compounds used for defense, signaling, and other functions. Industrially, diterpenes are used as natural aromas and flavoring, as pharmaceuticals, and as natural insecticides or repellents. Despite diterpene ubiquity in plant systems, it remains unknown how plants control diterpene localization and transport. For many other small molecules, plant cells maintain transport proteins that control compound compartmentalization. However, for most diterpene compounds, specific transport proteins have not been identified, and so it has been hypothesized that diterpenes may cross biological membranes passively. Through molecular simulation, we study membrane transport for three complex diterpenes from among the many made by members of the *Lamiaceae* family to determine their permeability coefficient across plasma membrane models. To facilitate accurate simulation, the intermolecular interactions for leubethanol, abietic acid, and sclareol were parametrized through the standard CHARMM methodology for incorporation into molecular simulations. To evaluate the effect of membrane composition on permeability, we simulate the three diterpenes in two membrane models derived from sorghum and yeast lipidomics data. We track permeation events within our unbiased simulations, and compare implied permeation coefficients with those calculated from Replica Exchange Umbrella Sampling calculations using the inhomogeneous solubility diffusion model. The diterpenes are observed to permeate freely through these membranes, indicating that a transport protein may not be needed to export these small molecules from plant cells. Moreover, the permeability is observed to be greater for plant-like membrane compositions when compared against animal-like membrane models. Increased permeability for diterpene molecules in plant membranes suggest that plants have tailored their membranes to facilitate low-energy transport processes for signaling molecules.

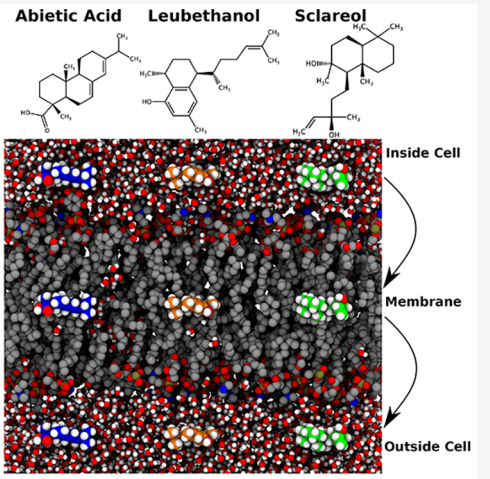

INTRODUCTION

Plants use a diverse range of molecules for protection and signaling to respond to pathogenic microorganisms and herbivores.[1,2] Diterpenes are phytoanticipin or phytoalexin compounds that plants produce for protection from a wide range of parasites and bacteria either in response to injury or as a preventative measure.[3] Diterpenes are a subclass of terpenoid compounds, synthesized from four isoprenoid diphosphate subunits. As a result, diterpenes are relatively large and complex, with 20 carbon atoms in diverse arrangements within the molecule.[4] Mechanistically, terpenoids can target bacterial enzymes,[5] bacterial biofilms,[6] and bacterial pigment formation,[7] act as bacterial toxins[8] and bacterial surfactants,[9] inhibit the quorum sensing pathways,[10] and inhibit microbial mobility.[11] Diterpenes also have other significant biological activities around plant growth regulation,[12] antimicrobial activity,[13] antiviral activity,[14] and algicidal applications.[15] This diversity in diterpene biological activity is enabled by the diverse diterpene structures produced in nature. The wide coverage of chemical space across naturally occurring plant diterpene is achieved by modularization of diterpene synthase (diTPS) enzymes and cytochrome P450-dependent monooxygenases (P450s).[4] The precursor geranylgeranyl diphosphate (GGPP) is converted into a wide range of diterpene metabolites by modular biosynthesis pathways.[4]

Received: October 13, 2022
Revised: January 6, 2023
Published: January 30, 2023

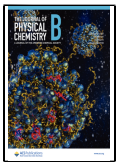

https://doi.org/10.1021/acs.jpcb.2c07209
J. Phys. Chem. B 2023, 127, 1144–1157

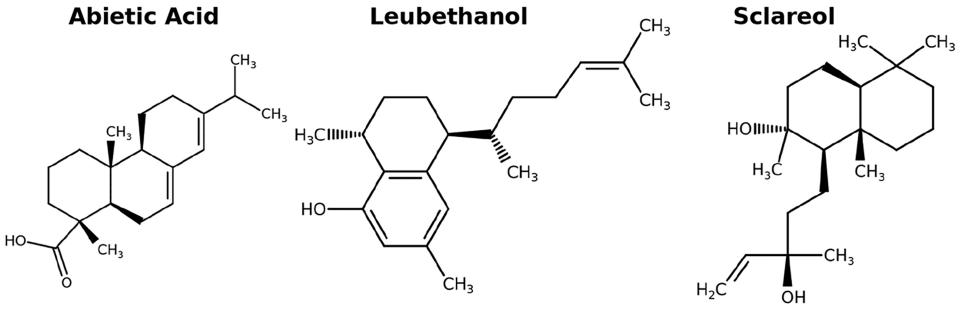

Figure 1. Chemical structures for the three diterpenes selected for the current permeability study, abietic acid, leubethanol, and sclareol.

Plant cells use passive[16] or regulated transport mechanisms[17] to move phytochemicals across lipid bilayers enveloping the cell or its subcellular compartments. In the wider literature, we can find a plethora of examples for regulated phytochemical transport through transporter proteins,[18] channels[19] and vesicular transport mechanisms[20] within plants. However, these transport mechanisms are highly specific. Transport proteins typically only recognize specific phytochemicals along with their close analogs. Channels, by contrast, are frequently specific to water or ion transport through gate mediated porins which span the membrane. Vesicular transport is most common for proteins and their products. Phytochemicals synthesized and secreted by plants have a very diverse range of chemical structure, which may preclude the transport mechanisms listed above. For some plant-derived compounds, such as the lignin found in plant cell walls, passive diffusion across cellular membranes without the need for a protein facilitator is supported by computational and experimental studies for fluxes across lipid bilayers.[21,22] The semipermiable cell membranes allows specific molecules to pass through depending on their chemical structure. In prior studies, cell plasma membranes are permeable to compounds which have a balance of aromatic and polar groups.[23,24] Diterpenes are similar to these compounds, exhibiting few polar groups and large hydrophobic cores (Figure 1). This characteristic structure for diterpene compounds may allow this class of compounds to permeate across the cell plasma membrane without the need for a membrane transport protein.

To test this hypothesis, we use classical molecular dynamics techniques to characterize permeation for three diterpene molecules, abietic acid, leubethanol, and sclareol (Figure 1), standing in for the highly diverse set of identified diterpenoids.[25] Sclaerol in particular piqued our interest, as its synthesis pathway is well characterized,[26] and prior studies had indicated that elevated sclaerol levels induced the expression of an ABC1 transporter protein in *Nicotiana plumbaginifolia*.[27] While sclareol induced expression, no further evidence was found for sclareol transport activity by the ABC transporter in subsequent studies,[28,29] leaving the transport mechanism unresolved. Abietic acid and leubethanol are other diterpenes that were tractable to parametrize based on a selection seen in plants,[30] with recent research highlighting their biosynthesis pathways.[31,32] Diterpenes in Figure 1 extend prior simulation studies, which demonstrated that terpenoids are permeable across model yeast plasma membranes.[33]

Unlike prior studies for terpene permeation,[33] where the CHARMM General force field (CGenFF)[34] accurately represented the small molecules, the higher complexity for the selected diterpenes mandated parametrization prior to simulation. Following parametrization, classical molecular dynamics simulations at equilibrium and replica exchange umbrella sampling techniques were used to determine the permeability coefficients for these molecules across model membranes for sorghum and yeast. We find that the three diterpenes studied face no significant barriers when crossing the membrane, and they would be expected to permeate passively and equalize concentrations on both sides of the membrane. We also find that the permeation rates are noticeably faster for plant-like sorghum membranes, suggesting that perhaps plants have tailored their membranes to optimize terpenoid permeability.

METHODS

Methodologically, the study had three phases:

1. Parameterization for the diterpenes of interest from Figure 1.
2. Unbiased simulations to assess the equilibrium behavior for the diterpenes in yeast and sorghum models.
3. Biased simulations to quantify the free energy and diffusivity profiles to determine the permeability coefficients for the diterpenes under study.

The methods for each of the three phases are captured in the subsections to follow.

Diterpene Parameterization. Accurate modeling for small molecules within molecular simulation requires describing the atomic interactions for the molecule with its surroundings. In classical molecular dynamics simulations, the underlying quantum mechanical (QM) potential energy surface is approximated with a force field,[35] where the energetic contributions are decomposed into pairwise and multibody interactions as follows:

$$
\begin{aligned}
U_{total} &= U_{non-bonded} + U_{bonded} \\
U_{total} &= (U_{VDW} + U_{electrostrostatic})_{non-bonded} + (U_{bonds} + U_{angles} + U_{dihedrals} + U_{impropers})_{bonded} \\
U_{total} &= \left(\left[\sum_{i,j} \epsilon_{i,j}\left(\left(\frac{R_{i,j}^{min}}{r_{i,j}}\right)^{12} - 2\left(\frac{R_{i,j}^{min}}{r_{i,j}}\right)^{6}\right)\right] + \left[\frac{q_i q_j}{4\pi\epsilon_0 r_{ij}}\right]\right) + \\
&\quad \left(\left[\sum_i k_i\left(b_i - b_0\right)^2\right] + \left[\sum_i k_i\left(a_i - a_0\right)^2 + k_i^{UB}\left(ub_i - ub_0\right)^2\right] + \right. \\
&\quad \left.\left[\sum_i k_i\left(1 + \cos(n_i\chi_i + \delta_i)\right)\right] + \left[\sum_i k_i\left(\chi_i - \chi_0\right)^2\right]\right)
\end{aligned}
\tag{1}
$$

In this representation, the total potential energy is split into pairwise nonbonded terms between all atom-pairs i and j and multibody terms to describe bonded interactions that occur between connected atoms. Since the forces acting on an atom are calculated from the gradient for this potential energy function, the motions and interactions between molecules are dependent on parameters set that describe the underlying potential energy landscape. Within the representation formulated by eq 1, free parameters include ϵ, R^{min}, and atomic

https://doi.org/10.1021/acs.jpcb.2c07209
J. Phys. Chem. B 2023, 127, 1144−1157

partial charges q within the nonbonded terms. Bonded terms are parametrized by a force constant k and equilibrium value represented in eq 1 with a subscripted 0. Oftentimes, these parameter sets can be drawn by analogy from existing parameters, using tools such as ParamChem.[34,36] However, when the molecular topology differs substantially from analogous terms already available in the force field, further refinement is needed.

Initial geometries for the three diterpene molecules from Figure 1, abietic acid, leubethanol and sclareol, were obtained from PubChem,[37] and checked for the correct stereochemistry. The starting geometries were used to determine analogous starting parameters within CGenFF[35] using the ParamChem Web server.[34,36] While the analogy for leubethanol was adequate, and could be used without further adjustment, abietic acid and sclareol required further parameter refinement. FFparam was utilized to implement the existing CHARMM parametrization protocol to optimize partial charges and bonded parameters.[38] Geometry optimization from the initial models was carried out using the MP2/6-31G* basis set using Gaussian 16 C.01.[39] The Merz−Singh−Kollman (MK) scheme was used to generate electrostatic derived potentials[40,41] for geometry optimization.

Following standard CHARMM parametrization procedures, partial atomic charges were optimized using quantum-derived water-interaction energies and geometries. Within these calculations, a water molecule is placed in favorable orientations with respect to hydrogen bond donors and acceptors on the small molecule, and restrained along the line for the putative hydrogen bond to determine the optimal interaction energy and distance. The water interaction calculations were carried out at the HF/6-31G* level of theory. QM target data to determine the bonded parameters were calculated using MP2/6-31G* level of theory, and bonded parameters for dihedrals for nonring atoms were scanned for 360° with 10° steps.

Output from the QM calculations were parsed into FFparam to build classical molecular mechanics (MM) systems to optimize parameters from eq 1. CHARMM36 was utilized for running the MM calculations in this step.[42] The Monte Carlo simulated annealing (MCSA) algorithm implemented in FFparam was used to optimize partial charges. Further manual fine-tuning was done to reduce the error gap in the interaction energy between MM and QM results, consistent with common partial charges for similar functional groups across the CHARMM force field. Autofitting the bonded parameters to minimize differences between QM and MM energies for equivalent geometries used LSFITPAR[43] together with some manual refinements to scale the terms to match others in the larger CHARMM force field ecosystem. The resulting topology and parameter files are provided as Supporting Information.

Unbiased Simulation for Diterpene Permeation. *Molecular System Assembly.* As a test for our parameters, and to have a general understanding for how the three tested diterpenes (Figure 1) would behave in a membrane environment, we developed two distinct membrane models. One model is identical with the yeast model used in prior terpenoid permeation simulations.[33] Each leaflet for the yeast membrane was comprised of a 30:14:9:9:4:1 ratio for phosphatidyl choline (PC), phosphatidyl ethanolamine (PE), phosphatidyl inositol (PI), ergosterol, phosphatidyl serine (PS), and phosphatidic acid (PA) headgroups, based on prior lipidomics work.[44−47] This is consistent with the yeast composition for a previous study on terpenoid permeation across yeast membranes.[33] Similarly, the sorghum headgroup composition was a 35:25:23:12:6:2:2 ratio for PC, digalactosyl diacylglycerol (DGDG), monogalactosyl diacylglycerol (MGDG), PE, sterols, phosphatidyl glycerol (PG), and PS, respectively, based on available lipidomics data.[48] The sterol component within the sorghum membrane was split in a 3:2:1 ratio between palmitoyl sitosteryl glucoside, palmitoyl campesteryl glucoside, and palmitoyl stigmasteryl glucoside, respectively.[48] While it is well-known that real biological membranes are generally asymmetric,[49] available lipidomics data were not collected with sufficient spatial resolution to distinguish between the leaflets. Therefore, lipids and sterols were symmetrically distributed in the two leaflets of the bilayer. The fully detailed composition for both the model yeast and sorghum membranes are presented in Table 1.

The membrane compositions for the yeast and sorghum membranes from Table 1 were constructed using the CHARMM-GUI web interface (Figure 2).[50] Six total simulation systems were generated, one for each possible diterpene-membrane combination. Within each system, 20 copies for a given diterpene were inserted in the system, ten initially above the membrane and ten below the membrane using the TopoTools module within VMD.[51,52] The diterpenes placed in solution were displaced at 35 Å away from the membrane center. Each system was solvated using the TIP3 water model through the solvate plugin within VMD.[52] Counterions were added to neutralize the system and add an extra 150 mM concentration of NaCl using the autoionize plugin in VMD.[52] Once complete, the yeast and sorghum simulation systems were approximately 90 Å and 80 Å long along the membrane surface. Since sorghum has larger glycolipid molecules, the simulation box was 115 Å tall in the membrane normal dimension, while the yeast membrane was 100 Å tall. In total, the simulation systems contained approximately 74,000 atoms and 67,000 atoms in yeast and sorghum simulation systems, respectively, at a diterpene concentration of approximately 50 mM.

The protonation states assigned to the membrane components were consistent with pH 7. At this pH, abietic acid is generally deprotonated and carries a formal negative charge, as the pK_a for abietic acid is around 4.7.[53] However, prior experimental[54] and computational approaches[22,55,56] have found that the neutral acid rather than the deprotonated carboxylate is the major species that crosses the hydrophobic membrane interior. Since the permeability coefficients for compounds with a carboxylate group can be 8−12 orders of magnitude slower than the neutral carboxylic acid,[22?] the largest share of the permeants will be the neutral form, as carboxylate forms of small molecules are only 100−1000 times more abundant at pH 7. Thus, all simulations carried out in this study use the neutral form for abietic acid, rather than the conjugate base abietate, consistent with the structure shown in Figure 1.

Simulation Protocol. To gain insight into the permeability mechanics at an atomic level, classical molecular dynamics simulation is utilized to determine what if any diterpene flux can be measured across the membrane. Simulations were carried out using the CHARMM36 force field for lipids,[57] together with CGenFF[35] and our reparameterization results to model the diterpene interactions. The TIP3 water model was used for the explicit solvent model.[58] A combination of NAMD 2.14 and NAMD 3.0a9 was used as the molecular dynamics

https://doi.org/10.1021/acs.jpcb.2c07209
J. Phys. Chem. B 2023, 127, 1144−1157

Table 1. Head Group and Tail Composition of One Leaflet of Yeast and Sorghum Bilayer Used for Equilibration and Steered Molecular Dynamics (SMD) Simulation

		yeast		sorghum	
lipid head groups	tails	equilibration	SMD	equilibration	SMD
PC	16:0−18:1	16	8	3	1
	16:0−18:2	–	–	12	4
	16:0−18:3	–	–	8	3
	18:1−18:1	7	4	–	–
	18:0−18:2	7	4	1	–
	18:2−18:2	–	–	8	3
	18:2−18:3	–	–	3	1
PE	16:0−18:1	8	4	1	–
	16:0−18:2	–	–	6	2
	16:0−18:3	–	–	2	1
	18:1−18:1	3	2	–	–
	18:0−18:2	3	2	–	–
	18:2−18:2	–	–	2	1
	18:2−18:3	–	–	1	–
PS	16:0−18:1	2	1	–	–
	16:0−18:2	–	–	1	–
	18:1−18:1	1	1	–	–
	18:0−18:2	1	1	–	–
	20:1−20:1	–	–	1	–
PA	16:0−18:1	1	1	–	–
PI	16:0−18:1	6	3	–	–
	16:0−18:2	3	2	–	–
PG	16:0−16:0	–	–	1	–
	16:0−18:2	–	–	1	–
DGDG	16:0−18:1	–	–	2	1
	16:0−18:2	–	–	11	4
	16:0−18:3	–	–	7	3
	18:0−18:2	–	–	1	–
	16:0−20:4	–	–	1	–
	18:2−18:3	–	–	1	–
	18:3−18:3	–	–	2	1
MGDG	16:0−18:1	–	–	3	1
	16:0−18:2	–	–	6	2
	16:0−18:3	–	–	3	1
	18:0−18:2	–	–	1	–
	16:0−20:4	–	–	2	1
	18:2−18:3	–	–	2	1
	18:3−18:3	–	–	6	3
sterols		18	4	6	2

engine, with NAMD 2.14 used for minimization while the GPU-resident integrator in NAMD 3.0a9 was used for production simulations to maximize performance.[59] Pressure was maintained using the Langevin piston model at 1 atm[60] with periodic cell growth. Temperature was kept constant at 298 K using the Langevin thermostat with 1 ps^{-1} damping. Hydrogen bonds lengths were fixed with SETTLE algorithm to enable a 2 fs time step.[61] Particle mesh Ewald (PME) grid was used to determine long-range electrostatic interactions with grid spacing of 1.2 Å.[62,63] Short range nonbonded terms were calculated with a 12 Å cutoff. Initially every system was minimized using 1000 steps of conjugate gradient in NAMD.[64] Then the system was equilibrated for 50 ps in an NPT ensemble using a 5 Å margin to allow the box size to vary significantly. Production simulations were run for 1000 ns with the default margin.

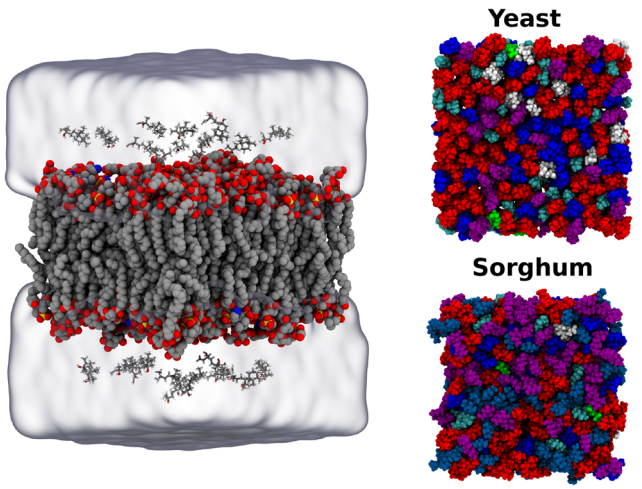

Figure 2. (Left) A representative starting configuration to begin simulation the starting distribution of diterpenes around the bilayer. The glass bubble representation shows the solution area. The diterpene is represented in licorice representation above and below the membrane, and bilayer heavy atoms are portrayed as beads, with the hydrogens omitted for visual clarity. (Right) A top view for the headgroup distribution within the sorghum and yeast lipid membranes. Each headgroup in this view has a unique color, red for PC, blue for PE, green for PA (in yeast) or PG (in sorghum), white for PS, purple for PI (in yeast) or DGDG (in sorghum), light blue for MGDG (in sorghum), and cyan for sterols.

Analysis. The data from molecular dynamics simulation was visualized and analyzed using python enabled VMD 1.9.4a48.[52] Python enabled VMD provides access to the numerical libraries of numpy and ploting tools like matplotlib.[65,66] One quantity of interest is the height along the membrane normal for the diterpene molecule center of mass, focusing on the bulkier cyclic moieties. Interditerpene contacts, diterpene membrane contacts and diterpene water contacts were calculated through a coordination number, evaluating atoms pairs within 5 Å of diterpene and then aggregating the distance-weighted contact function (eq 2).

$$C^{ij} = \sum_{i=1,j=1}^{n} \frac{1}{1 + e^{5(d^{ij}-4\text{Å})}} \tag{2}$$

Here C^{ij} is the matrix element quantifying the contacts between membrane atoms and diterpenes, i and j represent the indices for paired atoms from which a distance d^{ij} is computed over n saved trajectory snapshots. Equation 2 was originally derived to define native contacts;[67] however, this functional form has proved versatile for quantifying close contacts in a number of biological systems.[68−71]

Computing Permeability Coefficients through the Inhomogeneous Solubility Diffusion Model. We found few spontaneous permeation events where the molecule crossed from aqueous solution from one side of the membrane to the other. Thus, we could not use counting approaches to compute a permeability coefficient.[72] Instead, we calculated permeability coefficients directly from the inhomogeneous solubility diffusion model.[73−75] To facilitate this approach, we complemented our equilibrium simulations with nonequilibrium simulations to compute the free energy and diffusivity profiles along the membrane normal for these diterpenes. Following literature recommendations[55] and past experience,[22,33,56] we first used steered molecular dynamics to

https://doi.org/10.1021/acs.jpcb.2c07209
J. Phys. Chem. B 2023, 127, 1144−1157

generate diterpene configurations across the membrane, and subsequently exhaustively sample the membrane normal reaction coordinate using replica exchange umbrella sampling (REUS) calculations.[76]

Steered Molecular Dynamics. The steered molecular dynamics protocol used to seed the initial positions needed for REUS was done through a phased approach (Figure 3), analogous to previously published approaches.[22,33,56] In this system, only two diterpenes were present, as represented in Figure 3, each initially placed 45 Å away from the membrane center. Since the number of potential insertion elements is reduced, the systems used are substantially smaller to reduce computational cost, with a bilayer that is approximately 40% of the size used during equilibration simulation (Table 1). Through the colvars module,[77] two isolated diterpenes were either constrained or pulled across the membrane in successive simulations. To do so, the diterpenes molecules were held at a particular distance from the membrane midplane by a 5 kcal mol^{-1} Å^{-2} force constant applied to diterpene ring carbons. The diterpenes molecules were moved in two phases (Figure 3). In the first phase, one diterpene was moved toward the bilayer center over 15 ns. In the second phase, both diterpenes were moved in the same direction, inserting one molecule into the membrane while moving the other back into solution.

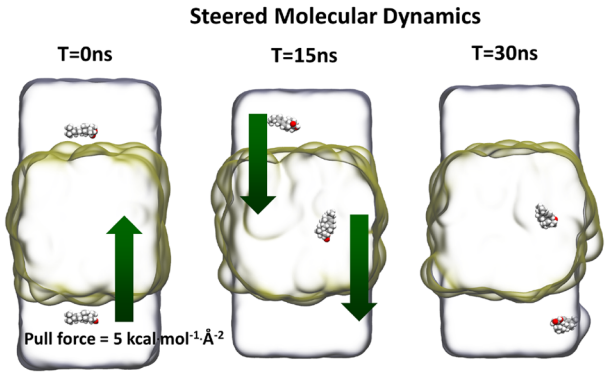

Figure 3. Pulling of diterpenes molecules using the steered molecular dynamics toward the center and then pulling them back out using 5 kcal mol^{-1} Å^{-2} of force constant.

States from the 15 ns second phase are used to seed the REUS calculations.

Replica Exchange Umbrella Sampling. The REUS simulations were conducted using 80 replicas with a force constant of 4 kcal mol^{-1} to restrain each diterpene independently on equally distributed umbrellas from [−45, 0] and [0, 45] Å from the membrane center. Each replicate was run for 50 ns, yielding 80 μs of effective sampling from which we can calculate permeability. Exchange between adjacent replicas was carried out every picosecond, with exchange ratios near the 20% optimum.[78]

The passive permeation of terpenoids can be quantified in terms of the permeability coefficient (Pm). Permeability for a molecule across a membrane can be described as molecular flux (J) over a concentration gradient (ΔC) and surface area (A) between two compartments ($J = \mathrm{Pm}\Delta CA$), based on Fick's law. To estimate Pm from the MD simulation, we applied the inhomogeneous solubility diffusion model.[73,74]

$$\mathrm{Pm} = \left[\int_{\xi_l}^{\xi_u} \frac{\exp(\Delta G(\xi)\beta)}{D(\xi)}\, \mathrm{d}\xi\right]^{-1} \tag{3}$$

Based on this model, the membrane permeability (Pm) depends only on the free energy profile relative to a chosen reference state (ΔG) and local diffusion profile (D) integrated along a reaction coordinate ξ between upper (ξ_u) and lower (ξ_l) bound of permeation end points. In order to compare with other studies, the upper and lower bound for the permeation end points are in solution. However, since the test compounds are quite lipophilic, by changing the integration boundaries within eq 3, it is possible to subdivide the permeability into crossing and extraction steps.[22,33] Since we computed a free energy profile, we also can independently estimate the partition coefficient (P) for terpenoids between the membrane and aqueous solution.

$$\log P = \frac{G_{aq} - G_{membrane}}{RT\ \ln 10} = \frac{\Delta G_{partition}}{RT\ \ln 10} \tag{4}$$

The free energy profile from the REUS trajectories were calculated from a modified version of Bayesian Weighted Histogram Analysis Method (BayesWHAM),[79] which uses Gibbs sampling of the known Dirichlet prior[80] to rapidly assess

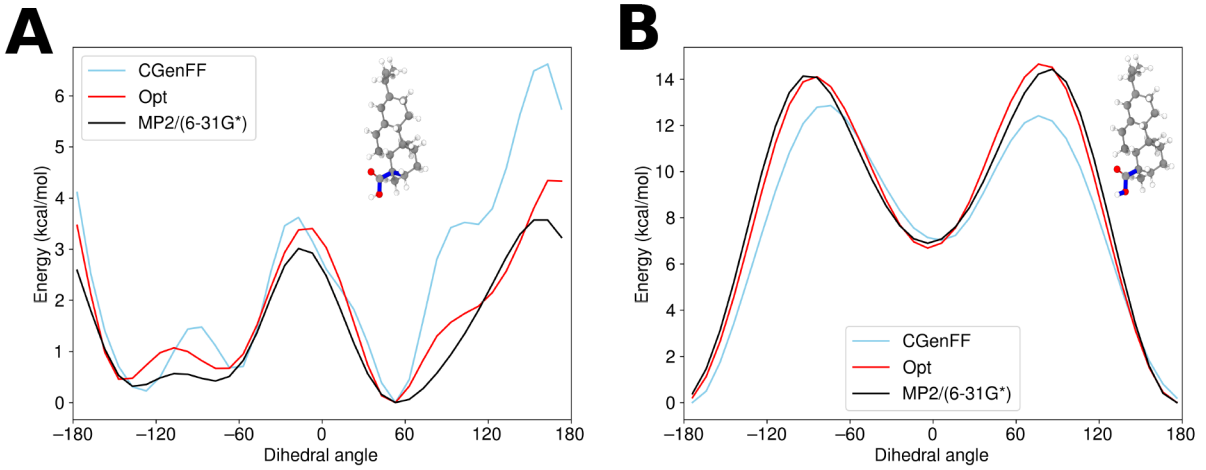

Figure 4. Dihedral free energy scans for abietic acid done by QM calculation (black), through CGenff parameters (light blue) and optimized parameters (red). The exact dihedral being optimized is highlighted in blue within the molecular structure shown as a plot inset.

https://doi.org/10.1021/acs.jpcb.2c07209
J. Phys. Chem. B 2023, 127, 1144−1157

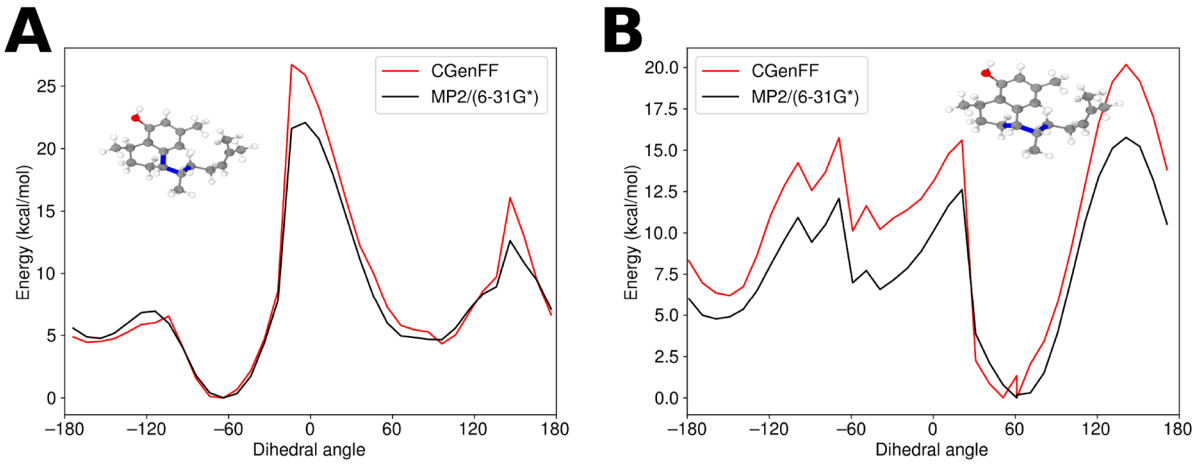

Figure 5. Dihedral free energy scans for leubethanol done by QM calculation (black) and through CGenff parameters (red). The exact dihedral scanned for energy profile is highlighted in blue within the molecular structure shown as a plot inset.

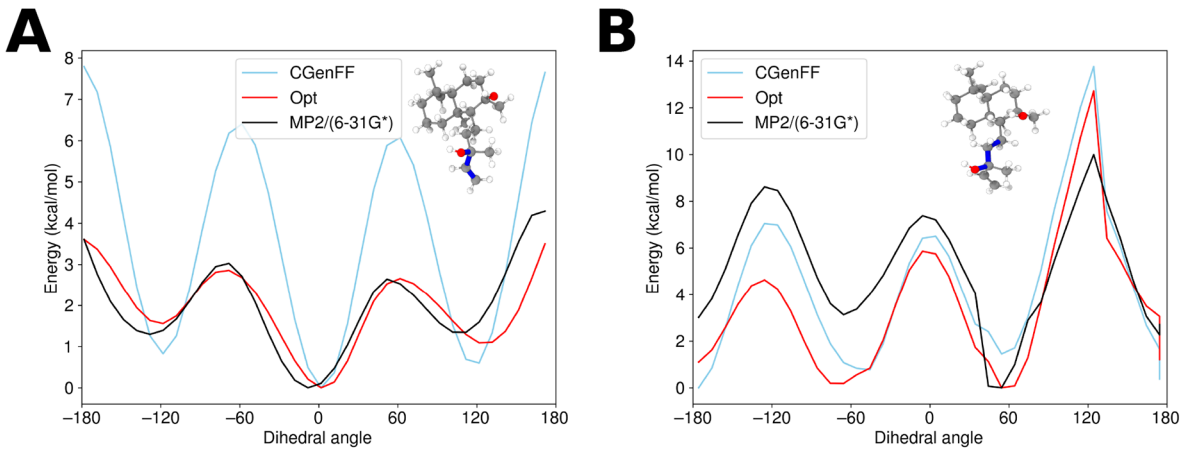

Figure 6. Dihedral free energy scans for sclareol done by QM calculation (black), through CGenff parameters (light blue) and optimized parameters (red). The exact dihedral being optimized is highlighted in blue within the molecular structure shown as a plot inset.

uncertainty. Diffusivity profiles for eq 3 were computed directly from the variance and autocorrelation time of the biased motion along the reaction coordinate.[81] This approach is less sensitive to the harmonic restraint force than the alternative calculation approaches,[82] and is independent of momentum removal around restarts.[83]

RESULTS

Estimating diterpene permeability from molecular mechanics required a systematic approach with the optimization of the molecular parameters for diterpene molecules. Optimized parameters allows us to study diterpene localization in a membrane environment through unbiased MD simulations. However, the underlying free energy landscape limits uniform efficient sampling, and so biased MD simulations were also performed to allow for a permeability coefficient to be calculated from eq 3.

Diterpene Parameterization. While the majority of steps taken to parametrize three diterpenes that are the focus of this study are detailed extensively as Supporting Information, we would like to highlight specific optimizations that have been improved substantially by refitting the parameters. Based on explicitly reparameterizing charges, our efforts improved the root mean squared error (RMSE) between QM and MM water interactions from approximately 1 kcal mol^{-1} to under a 0.27 kcal mol^{-1}, with leubethanol having the smallest RMSE at 0.12 kcal mol^{-1} (Tables S1−S3).

Due to the coupled rings within the diterpenes, explicit parametrization for all bonded terms was often missing. For abietic acid, the primary concern were dihedral terms related to rotation for the carboxylic acid relative to its connected ring (Figure 4A), which resulted in 6 coupled dihedral scans that could be fit simultaneously. CGenFF routinely overestimates the barrier for at least one rotation direction. While the results in Figure 4 indicate substantial improvement for problematic moieties, the initial CGenFF parameters captured most internal dynamics without reparameterization. We say this primarily by analyzing Figure 4B, where we reparameterize a hydroxyl rotation within the carboxylic acid moiety. While the penalty scores assigned by CGenFF are higher than ideal, the overall impact for reparameterization is small, indicating that the parameter analogy was good to start with. This provides us with confidence to not explicitly parametrize leubethanol, since energies computed through CGenFF substantially match the QM potential energy surface (Figure 5).

Sclareol provides an excellent counterexample where reparameterization was mandatory. The sclaerol features two coupled dihedrals (Figure 6). CGenFF appropriately treats one

https://doi.org/10.1021/acs.jpcb.2c07209
J. Phys. Chem. B 2023, 127, 1144−1157

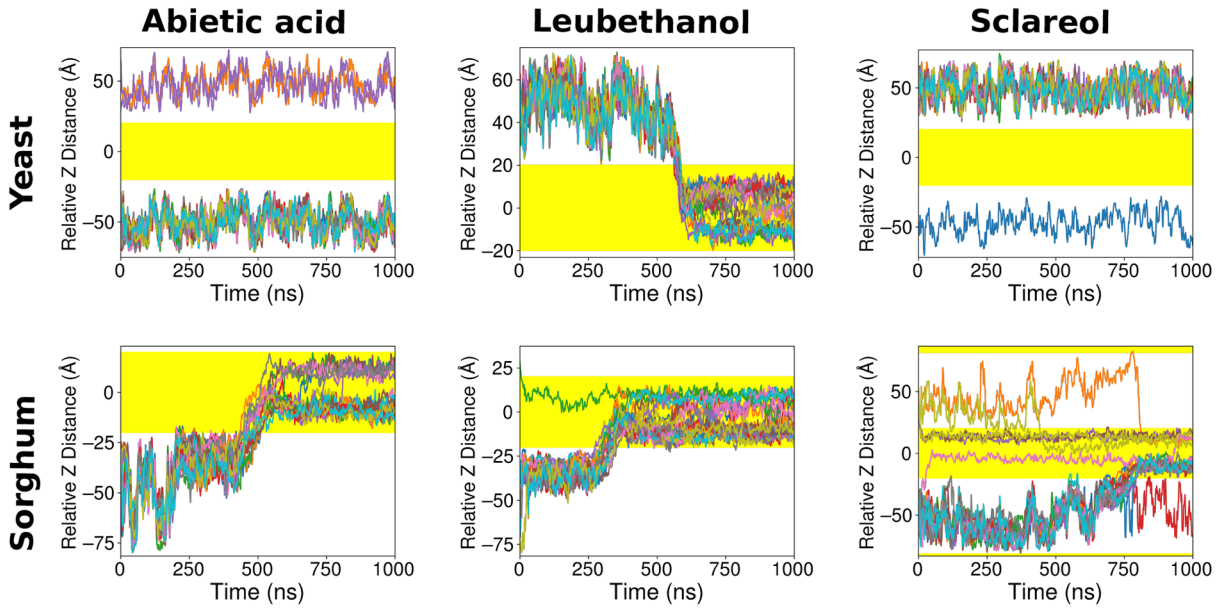

Figure 7. Trace plot for the position of each diterpene molecule, measured based on the geometric center for the rings, relative to the membrane center during equilibrium simulation. Since each system had 20 diterpenes (Figure 2), there are 20 lines with different colors representing the trace for an individual diterpene molecule. The trace has been unwrapped to eliminate discontinuities around the membrane normal dimension. The yellow shaded area represents the membrane extent, while the uncolored background represents the solvent.

dihedral, while overestimating energy barriers for the other dihedral substantially. However, since these dihedrals are coupled and were fitted simultaneously, we were only able to adequately parametrize one of these two scans. Thus, in an effort to reduce the error overall, our optimized parameters actually weaken the fit for one dihedral to vastly improve the fit for the coupled partner. We simultaneously fitted the two dihedral parameters together to reduce the error and our justifiable argument is that the barrier height around the energy minima are considerable enough that the MM result will represent the same conformation in energy minima state calculated through QM.

Diterpene Diffusion in Equilbration Trajectories. Classical MD simulation is an accurate and efficient method to study the membrane dynamics and simulate small molecule fluxes and interactions within a membrane environment. Small molecule behavior within these simulations is highly dependent on the empirical force field parametrized for MD simulation,[84] requiring significant effort to parametrize the selected diterpene molecules. Beyond calculating fluxes directly from potential membrane crossing events in equilibrium, unbiased simulation with multiple diterpene small molecules permits us to observe how our new diterpene parameters respond in a membrane environment. While we are most interested in the diterpene permeability in plant membranes, where diterpenes are naturally found, we also want to compare with previous simulation studies for diterpenes across yeast membranes.[33] Thus, two distinct membrane system were selected to compare diterpene diffusion across biological membranes, one from animal-like *Saccharomyces cerevisiae* membrane and another plant-like membrane from *Sorghum bicolor*. By comparing diffusion behavior and measured permeability across species, we can answer if larger terpenes cross biological membranes as readily as smaller terpenes do.[33]

Diterpene Aggregation and Membrane Insertion. The diterpenes from Figure 1 are largely lipophilic molecules, with only a few polar moieties. As such, diterpenes would be expected to easily permeate into the membrane.[85] To track diterpene permeation, the system was designed so that the *Z* axis was normal to membrane surface. With this construction, tracing the *Z*-coordinate for the small molecules relative to the membrane center would yield a metric for membrane insertion.

Plotting the relative *z*-distance between the membrane and individual diterpenes results in Figure 7. At equilibrium, the individual small molecules will cluster quickly, as seen from the aggregated lines in Figure 7. The diterpenes are observed to insert under certain conditions, and often will do so as a group. For instance, both leubethanol simulations see all the diterpene molecules inserted, regardless of membrane composition. The other two diterpene molecules will aggregate strongly, and the aggregates may never find their way into the membrane, particularly for the yeast membrane model.

From Figure 7, we find that diterpenes that do insert into the membrane cross at different rates, depending on diterpene chemistry and membrane composition. Tabulating interleaflet transfers for diterpene molecules, we find that leubethanol switches between leaflets more quickly in the sorghum model membrane than in the yeast-like membrane (Table S4). Leubethanol also demonstrates the most transit events across the three diterpenes tested. Chemically, the additional hydroxyl groups on abietic acid and sclareol would generally retard interleaflet exchange, as these groups would need to shed their hydration layer prior to membrane transit.

While we had anticipated that the insertion processes for individual diterpene molecules would be independent from one another, Figure 7 instead reveals that the insertion processes are coordinated. Diterpenes in solution are observed to aggregate together, leading to diterpene aggregates inserting as a collective rather than as individually soluble molecules (Figure 8). Aggregation for the diterpenes may be a real phenomenon, representing a scenario whereby the diterpenes or other small organics become soluble in water. In Figure 8,

https://doi.org/10.1021/acs.jpcb.2c07209
J. Phys. Chem. B 2023, 127, 1144−1157

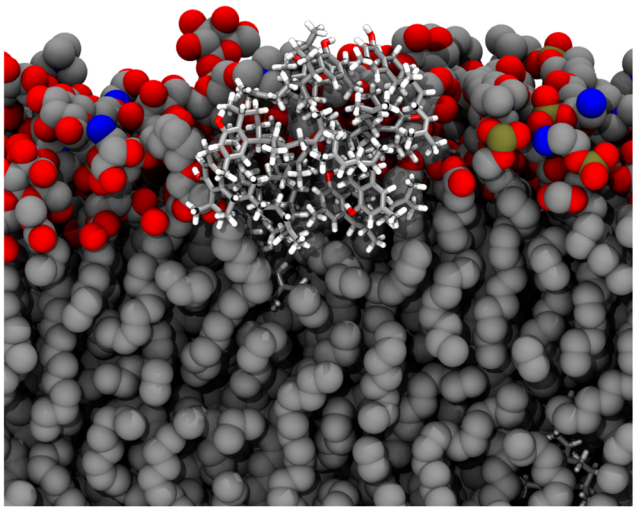

Figure 8. Snapshot highlighting leubethanol aggregation during the insertion process into the membrane bilayer. Licorice bond style representation depicts the leubethanol while beads represent the membrane bilayer. Membrane hydrogen atoms were hidden in this representation, and atoms are colored by element. Hydrogen, oxygen, nitrogen, carbon, and phosphorus are white, red, blue, gray, and tan, respectively.

we see that the polar groups within the leubethanol mass are exposed to the solvent, where they may form hydrogen bonds. Further stabilizing aggregated states are lipophilic contacts between diterpenes. If the polar groups on the diterpene are pushed toward the surface of aggregated diterpenes by lipophilic forces, they are able to form hydrogen bonds with the surrounding solvent.

Qualitatively, what is happening is a consequence for the poor solubility of diterpenes generally. Their hydrophobic bulk means that they are not normally miscible in water like a small solvent like ethanol might be. Since the individual molecules can diffuse rapidly, they find one another quickly within our small simulation volume. Thus, these aggregates form whenever the bulk water volume is sufficiently small such that the diterpenes are likely to find one another before insertion takes place, and may represent a mechanism by which the diterpenes are exported from the cell in large quantities.

We can quantify the aggregation further through contact analysis (Figure 9). In this instance, we observe that interditerpene contacts and diterpene contacts with water (Figure 9, parts A and B) decrease in conjunction with membrane insertion (Figure 7 and Figure 9C). After insertion, the pressure for the diterpenes to aggregate is strongly reduced, and most contacts are formed between diterpenes and the surrounding membrane lipids. The aggregation breakup is very fast, with interditerpene contacts being largely abolished within 100 ns or so of coming into contact with the membrane and beginning the insertion process.

The natural question is why sclareol does not follow this trend. Critically, sclareol has two hydroxyl groups, and it does form more hydrogen bonds than either abietic acid or leubethanol (Figure 9D). The pair of hydroxyl groups may facilitate more stable aggregates in solution, effectively hiding the hydrophobic core for scalerol behind favorable interactions with water. At lower concentrations, where aggregates cannot form, we may see a totally different insertion pattern than what we see from unbiased simulation.

Taking the same trajectories and analysis, we can compute a histogram for the diterpene distribution within our trajectories (Figure 10). Once inserted, the diterpenes are effectively randomly distributed laterally within the membrane, with potential asymmetries depending on the leaflet into which the aggregates inserted into first. The probability distribution peak with respect to the z axis is just below the head groups (Figure 10). In this orientation, the diterpene hydroxyls are able to hydrogen bond with lipid headgroups or water. For sclaerol, the aggregates are also very clear in this view, driven by the extra hydrogen bonds present in the simulation (Figure 9D). We also see the aggregate in water tends to stay away from the membrane which could be due to the hydrogen bonding by the polar groups in diterpenes.

From a permeability perspective, the equilibrium results are suboptimal. Aggregation interferes with insertion, and biases interleaflet exchanges by creating a large initial concentration gradient between both membrane leaflets. Thus, to quantify

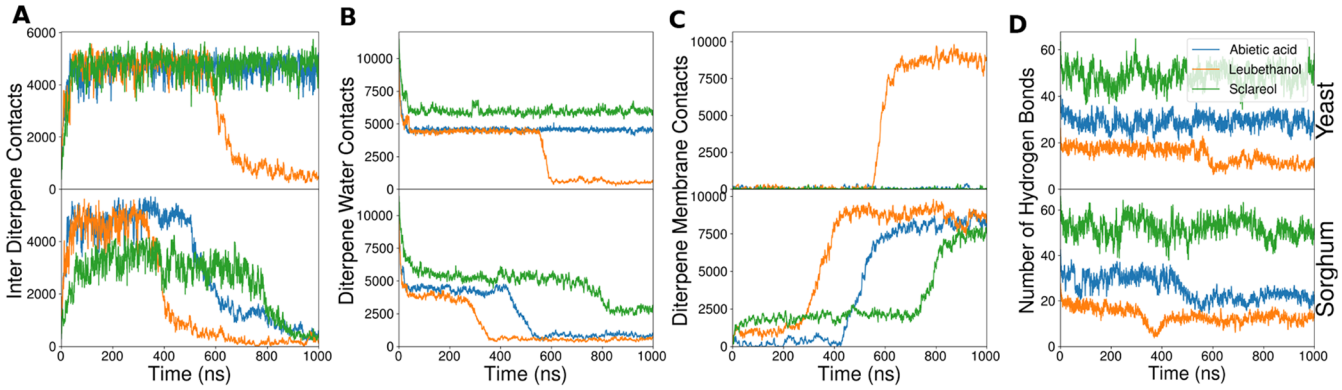

Figure 9. Quantification for plot for (A) interditerpene contacts, (B) water−diterpene contacts and (C) membrane−diterpene contacts, with the time series for different diterpenes in different colors. (D) Quantification of the hydrogen bonds formed by the diterpenes within the molecular environment. The interditerpene contact sum is determined by first computing the distance between diterpene heavy atoms that are not members of the same residue. The diterpene−water contact sum is determined by first computing the distance between diterpene heavy atoms and water oxygen atoms. The diterpene−membrane contact sum is determined by first computing the distance between diterpene and membrane heavy atoms. The distances are then weighted the distance-weighted contact function from eq 2, and the individual C values are summed together to yield the total contact number.

https://doi.org/10.1021/acs.jpcb.2c07209
J. Phys. Chem. B 2023, 127, 1144−1157

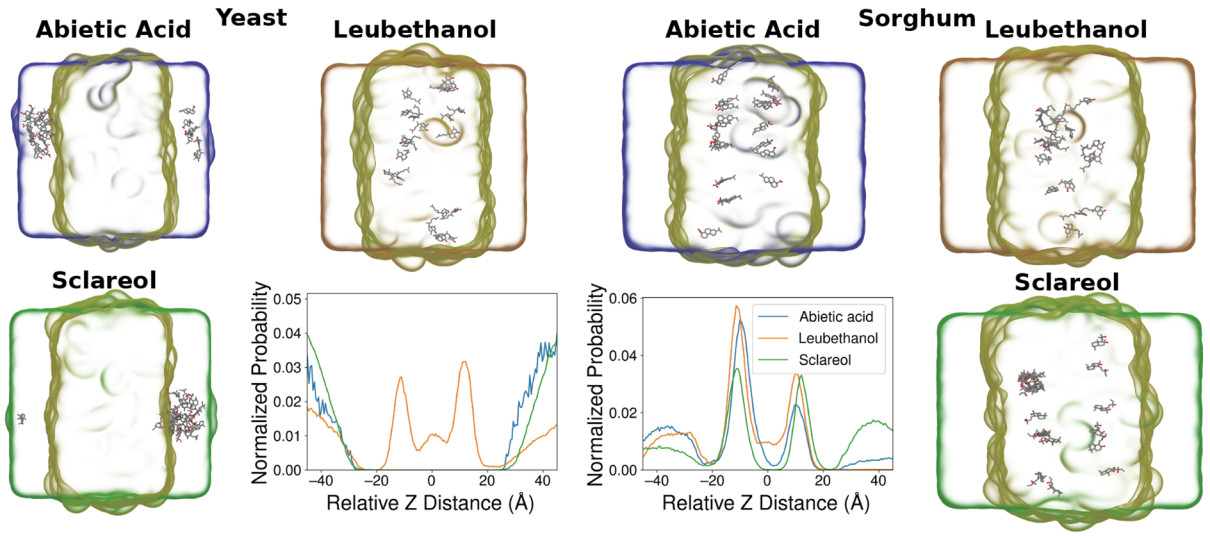

Figure 10. Normalized probability distribution of diterpenes in each equilibrated simulation system over the full 1 μs trajectory, together with diterpene snapshots within the simulation system representing the distribution of diterpenes at the end of 1 μs of equilibration trajectory. Colors blue, orange, and green represent the abietic acid, leubethanol, and sclareol, respectively.

permeability at lower diterpene concentrations that are more physiologically relevant, we also carry out REUS calculations.

Diterpene Partitioning and Permeability from REUS Simulations. The free energy landscape for diterpene motion across both sorghum and yeast membranes was sampled extensively through REUS simulations. Sampling the energy landscape in relatively small windows of 0.57 Å provided ample data to apply BayesWHAM[79] to estimate the free energy profile within the membrane environment. The estimated free energy profile showed very small error estimates, with the BayesWHAM approach estimating the uncertainty to be <0.02 kcal/mol based on statistical analysis. From the resulting free energy profile (Figure 11), diterpenes are observed to favorably partition into the membrane. The partitioning favors placing the diterpenes at the membrane−water interface, with the minima at approximately 12−15 Å. At this depth, the hydroxyl groups can hydrogen bond with lipid carbonyl and lipid headgroups, while shielding lipophillic groups from solution. As the molecules become more hydrophilic, such as sclareol with two hydroxyl groups as compared with one hydrophilic moiety for the other compounds, the favorability for the preferred membrane penetration depth is reduced. Likewise, the carboxylic acid on abietic acid is capable of making more water interactions than a single hydroxyl, raising the free energy minimum slightly.

Entering the membrane from solution is observed to have a minimal barrier, suggesting that isolated diterpenes can quickly find the free energy minimum rather than aggregate together as was observed here. Conversely, the barriers for crossing the membrane midplane vary considerably. Desolvating both hydroxyls raises the free energy at the membrane interior for sclareol relative to the other diterpenes. By comparison, interleaflet translocation is relatively low-cost, consistent with the observed interleaflet crossings observed from Figure 7.

The diffusion profiles needed to determine permeability through eq 3 are also found in Figure 11. What we observe is that diffusion is fastest in bulk solution, slower at the interface, and slower still in the membrane interior. This can be best understood from the diffusive behavior for the environment around the diterpene. Dilute aqueous environments have

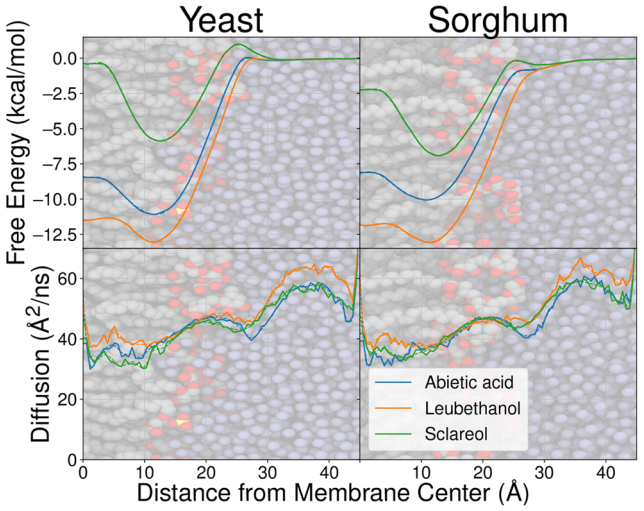

Figure 11. Free energy profile and local diffusivity for diterpenes compounds. For the free energy profile, the reference point was chosen to be the compound in aqueous solution (right), which transits the bilayer (center), and is eventually pulled into the center (left). Standard errors for the free energy profile are drawn as semitransparent regions, which are rarely visible outside of the main line. Each compound has two lines associated with the compound, a solid line reflecting the instantaneous best estimate for the quantity of interest and a dashed line indicating the spline fit used to numerically integrate eq 3 to tabulate permeability coefficients. As a visual aide, a simplified atomistic representation of the respective components is used as a background, with water oxygens and lipid heavy atoms following a standard color scheme (gray for carbons, red for oxygens in lipids, blue for the oxygen in water, and yellow for phosphorus).

higher diffusion coefficients than membrane environments generally. In membranes, motions are constrained by large acyl tails that prevent free diffusion. Only at the membrane midplane, where the most common chemical structures are the methyl termini for the acyl tails, is the diffusion coefficient seen to increase again.

Looking strictly at Figure 11, it is difficult to see a consistent difference between the yeast and sorghum membranes by eye

https://doi.org/10.1021/acs.jpcb.2c07209
J. Phys. Chem. B 2023, 127, 1144−1157

Table 2. Partition (P) and Permeability (Pm_e) Coefficients for Diterpenes in Yeast and Sorghum Membranes[a]

group	compound name	log P	$\log_{10}[Pm_e$ (cm s^{-1})]	$\log_{10}[Pm_c$ (cm s^{-1})]	$\log_{10}[Pm_{ex}$ (cm s^{-1})]
yeast	abietic acid	8.1	1.2	−0.4	−6.7
	leubethanol	9.6	1.2	0.2	−8.1
	sclareol	4.3	0.8	−2.4	−3.2
sorghum	abietic acid	7.4	1.3	0.1	−5.7
	leubethanol	9.6	1.4	0.5	−7.9
	sclareol	5.1	1.2	−1.8	−3.5

[a]The partitioning is based on difference in free energy for diterpenes in membrane and water (eq 4). Permeability is decomposed into a crossing permeability (Pm_c) and extraction permeability (Pm_{ex}). These permeabilities are calculated as discussed in methods by eq 3. The effective permeability coefficient (Pm_e) is calculated as $\log[Pm_e] = \log P + \log_{10}[(Pm_c^{-1} + 2Pm_{ex}^{-1})^{-1}]$, and represents the permeability coefficient for compounds from aqueous solution to aqueous solution through the membrane.

alone. The diffusion coefficients show similar trends for the three diterpenes tested. The order for the partitioning behavior is similar between the yeast and sorghum membranes, with generally small ($1-2$ kcal mol^{-1}) differences when comparing the free energy profile. The differences between the free energy profiles do not appear to be systematic, as the free energy minimum for abietic acid is lower in a animal-like yeast membrane, while the free energy minimum for sclareol is lower for a plant-like sorghum membrane. However, by applying eq 3 to calculate permeability, we can quantify how these small changes in behavior translate into permeability coefficients.

Partition and Permeability Coefficients. Permeability and partition coefficients are derived quantities from the free energy and diffusivity profiles from Figure 11, utilizing the inhomogeneous solubility diffusion model expressed in eq 4 and eq 3 detailed in the methods. Tabulating these quantities in Table 2, we find that the permeation coefficient measuring interleaflet transitions (Pm_c) is more positive for diterpenes in sorghum-like membranes, indicating that the interleaflet transition rates would be faster in this membrane environment. There is not a consistent trend for the rate at which diterpenes could be extracted from the membrane, or for the partition coefficients. However, the overall effect is that the effective permeability for sorghum membranes is 0.1−0.4 log units larger. Given the small uncertainties for the barrier heights in the free energy profile, the permeabilities in Table 2 are accurate to within 0.05 log units in the worst case, but they are more typically accurate to 0.02 log units. Thus, the measured differences stand statistical scrutiny as being significant.

To put this into context, the net flux (J) across a membrane with surface area A and concentration difference ΔC is given by

$$J = Pm_e A \Delta C \tag{5}$$

Thus, for the same concentration gradient across a cell membrane, diterpenes would cross the membrane 1.2−2.5× faster in sorghum than in yeast based strictly on the increased effective permeability coefficient. This raises the possibility that plants have optimized membrane compositions that increase diterpene permeability, facilitating diterpene movement within the plant. Fast diffusion across plant membranes would help diterpenes act as signaling molecules, such as in growth and defense contexts,[86,87] or potentially to facilitate modifying diterpenes once synthesized in the plastid.[88]

Considering the net flux equation, we can access how fast would the diterpenes diffuse out passively in plants, as the compounds would be generated by cellular metabolism and then wicked away by either transport processes within plants or transfer into the atmosphere. If we assume that the diterpene concentration is roughly on the order of 1 μmol/L, the permeability coefficients of approximately 10 cm/s implied by Table 2 would mean that the flux per unit area (J/A) would be on the order of 100 μmol m^{-2} s^{-1}. Taken over the membranes for a whole leaf or a whole plant, such a flux density would represent fast product export route, likely faster than what a diterpene-specific pump could provide.

Diterpenes in this study have been reported to have a minimum inhibitory concentration in the range of 20−50 μmol/L against a wide range of targets.[89−91] By rearranging eq 5, we see that maintaining a concentration gradient on the 1 μmol/L scale for a cell with roughly 2500 μm^2 of membrane surface area with a permeability coefficient of about 10 cm/s would require 250 fmol of these diterpene compounds to be pumped out of the cell every second, or about 150 billion molecules per second. Assuming transport protein turnover of 10 per second, this would clearly represent an overburdened transport system that cannot sustain such a large gradient. Thus, the observed minimum inhibitory concentration for these diterpenes are unlikely to represent acute toxicity when transport pumps exceed their capacity, as is the case for antibiotics and their associated resistance mechanisms. Instead, the observed growth inhibition at high diterpene concentrations may be a weaker allosteric effect across multiple targets or membrane disruption at sufficiently high concentration.

However, we need to return to the protonation state of abietic acid, which we took to be the neutral form. Given the pK_a of 4.7,[53] we would expect approximately 1 in every 200 abietate molecules to be protonated and form abietic acid at pH 7. Since the permeability for carboxylate-bearing molecules is expected to be very low by comparison based on prior investigations in lignin,[22,56] effectively only the neutral form will permeate at near-neutral pH. Thus, the effective permeability in Table 2 would be adjusted downward by a factor of 200 (2.3 log units), making it the slowest permeant out of the set. However, even with this reduced permeation, we predict that active transport would not be able to maintain a large abietate gradient.

CONCLUSION

This study was designed to probe the mechanistic underpinnings and kinetics for diterpene transport across biological membranes, utilizing sclareol, leubethanol, and abietic acid as representative stand-ins for diterpene compounds broadly. These compounds were parametrized according to the CHARMM parametrization scheme, and facilitated classical molecular dynamics simulations of membrane permeation for

https://doi.org/10.1021/acs.jpcb.2c07209
J. Phys. Chem. B 2023, 127, 1144−1157

diterpene compounds. Based on equilibrium simulation, we find that diterpenes quickly interchange between leaflets once the compounds are inserted, with the least oxygenated diterpene in our study (leubethanol) demonstrating the fastest interleaflet exchange. We also observe that diterpene aggregates at high concentration may be stable in solution for longer than anticipated, perhaps hinting at how oily substances such as waxes are deposited on leaf surfaces during plant development.

To quantify the energetics and permeability for isolated diterpenes through biological membranes, we utilized biased simulations using REUS coupled to the inhomogeneous solubility diffusion model. We find minimal energetic barriers for diterpene entry into either membrane, and broadly similar free energy profiles across the membrane span for both plant-like sorghum membrane and animal-like yeast membrane models. While the energetics are largely similar between the two membrane models, the resulting permeabilities are very high, suggesting that active transport processes would not be able to maintain even a small concentration gradient across the membrane over the long-term. Interestingly, computed permeability coefficients for diterpenes across plant membranes are consistently larger, suggesting that plants may have coevolved their membrane composition to optimize permeability for these key signaling and defense compounds.

■ ASSOCIATED CONTENT

Data Availability Statement

All input scripts to build and run molecular simulations are made publicly available on Zenodo.[92]

Supporting Information

The Supporting Information is available free of charge at https://pubs.acs.org/doi/10.1021/acs.jpcb.2c07209.

CHARMM-format topology and parameter files for the compounds of interest (ZIP)

An extended methods section describing the parametrization process for the three diterpenes considered here, as well as quantification for the number of crossing events observed during simulation (PDF)

■ AUTHOR INFORMATION

Corresponding Author

Josh V. Vermaas − *Plant Research Laboratory, College of Natural Science, Michigan State University, East Lansing, Michigan 48824, United States; Department Of Biochemistry and Molecular Biology, College of Natural Science, Michigan State University, East Lansing, Michigan 48824, United States;* orcid.org/0000-0003-3139-6469; Phone: +1 (517) 884-6937; Email: vermaasj@msu.edu

Authors

Saad Raza − *Plant Research Laboratory, College of Natural Science, Michigan State University, East Lansing, Michigan 48824, United States;* orcid.org/0000-0003-4842-2192

Mykayla Miller − *Department of Chemistry and Biochemistry, California State University, Fullerton, Fullerton, California 92831, United States*

Björn Hamberger − *Department Of Biochemistry and Molecular Biology, College of Natural Science, Michigan State University, East Lansing, Michigan 48824, United States;* orcid.org/0000-0003-1249-1807

Complete contact information is available at: https://pubs.acs.org/10.1021/acs.jpcb.2c07209

Notes

The authors declare no competing financial interest.

■ ACKNOWLEDGMENTS

M.M. was supported under the Summer Research Opportunities Program (SROP) at Michigan State University. B.H. acknowledges the US Department of Energy Great Lakes Bioenergy Research Center Cooperative Agreement DE-SC0018409. We acknowledge support from the Institute for Cyber Enabled Research (ICER) at MSU, which provided the computing resources utilized for this project. This work used the Extreme Science and Engineering Discovery Environment (XSEDE), which is supported by National Science Foundation Grant Number ACI-1548562[93] (Project Number TG-BIO210040).

■ REFERENCES

(1) Hunziker, P.; Lambertz, S. K.; Weber, K.; Crocoll, C.; Halkier, B. A.; Schulz, A. Herbivore feeding preference corroborates optimal defense theory for specialized metabolites within plants. *Proc. Natl. Acad. Sci. U. S. A.* **2021**, *118*, No. e2111977118.

(2) Hammerbacher, A.; Coutinho, T. A.; Gershenzon, J. Roles of plant volatiles in defence against microbial pathogens and microbial exploitation of volatiles. *Plant, Cell & Environment* **2019**, *42*, 2827−2843.

(3) Silva, L. N.; Zimmer, K. R.; Macedo, A. J.; Trentin, D. S. Plant natural products targeting bacterial virulence factors. *Chem. Rev.* **2016**, *116*, 9162−9236.

(4) Andersen-Ranberg, J.; Kongstad, K. T.; Nielsen, M. T.; Jensen, N. B.; Pateraki, I.; Bach, S. S.; Hamberger, B.; Zerbe, P.; Staerk, D.; Bohlmann, J.; et al. Expanding the landscape of diterpene structural diversity through stereochemically controlled combinatorial biosynthesis. *Angew. Chem., Int. Ed.* **2016**, *55*, 2142−2146.

(5) Kim, J. H.; Ryu, Y. B.; Lee, W. S.; Kim, Y. H. Neuraminidase inhibitory activities of quaternary isoquinoline alkaloids from Corydalis turtschaninovii rhizome. *Bioorg. Med. Chem.* **2014**, *22*, 6047−6052.

(6) Carneiro, V. A.; Santos, H. S. d.; Arruda, F. V. S.; Bandeira, P. N.; Albuquerque, M. R. J. R.; Pereira, M. O.; Henriques, M.; Cavada, B. S.; Teixeira, E. H. Casbane diterpene as a promising natural antimicrobial agent against biofilm-associated infections. *Molecules* **2011**, *16*, 190−201.

(7) Pejin, B.; Ciric, A.; Glamoclija, J.; Nikolic, M.; Sokovic, M. In vitro anti-quorum sensing activity of phytol. *Natural product research* **2015**, *29*, 374−377.

(8) Li, H.-e.; Qiu, J.-z.; Yang, Z.-q.; Dong, J.; Wang, J.-f.; Luo, M.-j.; Pan, J.; Dai, X.-h.; Zhang, Y.; Song, B.-l.; et al. Glycyrrhetinic acid protects mice from *Staphylococcus aureus* pneumonia. *Fitoterapia* **2012**, *83*, 241−248.

(9) Mafud, A. C.; Silva, M. P.; Monteiro, D. C.; Oliveira, M. F.; Resende, J. G.; Coelho, M. L.; de Sousa, D. P.; Mendonça, R. Z.; Pinto, P. L.; Freitas, R. M.; et al. Structural parameters, molecular properties, and biological evaluation of some terpenes targeting *Schistosoma mansoni* parasite. *Chemico-Biological Interactions* **2016**, *244*, 129−139.

(10) Cugini, C.; Calfee, M. W.; Farrow, J. M., III; Morales, D. K.; Pesci, E. C.; Hogan, D. A. Farnesol, a common sesquiterpene, inhibits PQS production in *Pseudomonas aeruginosa*. *Molecular microbiology* **2007**, *65*, 896−906.

(11) Annapoorani, A.; Umamageswaran, V.; Parameswari, R.; Pandian, S. K.; Ravi, A. V. Computational discovery of putative quorum sensing inhibitors against LasR and RhlR receptor proteins of *Pseudomonas aeruginosa*. *Journal of computer-aided molecular design* **2012**, *26*, 1067−1077.

(12) Hanson, J. The chemistry of the gibberellins. *Natural Product Reports* **1990**, *7*, 41−59.
(13) Zhu, C.; Xu, B.; Adpressa, D. A.; Rudolf, J. D.; Loesgen, S. Discovery and biosynthesis of a structurally dynamic antibacterial diterpenoid. *Angew. Chem., Int. Ed.* **2021**, *60*, 14163−14170.
(14) Yamamoto, T.; Izumi, N.; Ui, H.; Sueki, A.; Masuma, R.; Nonaka, K.; Hirose, T.; Sunazuka, T.; Nagai, T.; Yamada, H.; et al. Wickerols A and B: novel anti-influenza virus diterpenes produced by *Trichoderma atroviride* FKI-3849. *Tetrahedron* **2012**, *68*, 9267−9271.
(15) Waridel, P.; Wolfender, J.-L.; Lachavanne, J.-B.; Hostettmann, K. ent-Labdane diterpenes from the aquatic plant *Potamogeton pectinatus*. *Phytochemistry* **2003**, *64*, 1309−1317.
(16) Tomkins, M.; Hughes, A.; Morris, R. J. An update on passive transport in and out of plant cells. *Plant Physiology* **2021**, *187*, 1973−1984.
(17) Grotewold, E. The challenges of moving chemicals within and out of cells: insights into the transport of plant natural products. *Planta* **2004**, *219*, 906−909.
(18) Dixon, D. P.; Lapthorn, A.; Edwards, R. Plant glutathione transferases. *Genome biology* **2002**, *3*, reviews3004.1.
(19) Barton, D. A.; Cole, L.; Collings, D. A.; Liu, D. Y.; Smith, P. M.; Day, D. A.; Overall, R. L. Cell-to-cell transport via the lumen of the endoplasmic reticulum. *Plant Journal* **2011**, *66*, 806−817.
(20) Lazzaro, M.; Thomson, W. The vacuolar-tubular continuum in living trichomes of chickpea (*Cicer arietinum*) provides a rapid means of solute delivery from base to tip. *Protoplasma* **1996**, *193*, 181−190.
(21) Perkins, M. L.; Schuetz, M.; Unda, F.; Chen, K. T.; Bally, M. B.; Kulkarni, J. A.; Yan, Y.; Pico, J.; Castellarin, S. D.; Mansfield, S. D.; et al. Monolignol export by diffusion down a polymerization-induced concentration gradient. *Plant Cell* **2022**, *34*, 2080−2095.
(22) Vermaas, J. V.; Dixon, R. A.; Chen, F.; Mansfield, S. D.; Boerjan, W.; Ralph, J.; Crowley, M. F.; Beckham, G. T. Passive membrane transport of lignin-related compounds. *Proc. Natl. Acad. Sci. U. S. A.* **2019**, *116*, 23117−23123.
(23) Lipinski, C. A.; Lombardo, F.; Dominy, B. W.; Feeney, P. J. Experimental and computational approaches to estimate solubility and permeability in drug discovery and development settings. *Advanced drug delivery reviews* **1997**, *23*, 3−25.
(24) Yang, N. J.; Hinner, M. J. Getting across the cell membrane: an overview for small molecules, peptides, and proteins. *Site-specific protein labeling* **2015**, *1266*, 29−53.
(25) Shen, Y.; Liang, W.-J.; Shi, Y.-N.; Kennelly, E. J.; Zhao, D.-K. Structural diversity, bioactivities, and biosynthesis of natural diterpenoid alkaloids. *Natural Product Reports* **2020**, *37*, 763−796.
(26) Chalvin, C.; Drevensek, S.; Gilard, F.; Mauve, C.; Chollet, C.; Morin, H.; Nicol, E.; Héripré, E.; Kriegshauser, L.; Gakière, B.; et al. Sclareol and linalyl acetate are produced by glandular trichomes through the MEP pathway. *Horticulture research* **2021**, *8*, 206.
(27) Jasiński, M.; Stukkens, Y.; Degand, H.; Purnelle, B.; Marchand-Brynaert, J.; Boutry, M. A plant plasma membrane ATP binding cassette−type transporter is involved in antifungal terpenoid secretion. *Plant Cell* **2001**, *13*, 1095−1107.
(28) van den Brûle, S.; Smart, C. C. The plant PDR family of ABC transporters. *Planta* **2002**, *216*, 95−106.
(29) Campbell, E. J.; Schenk, P. M.; Kazan, K.; Penninckx, I. A.; Anderson, J. P.; Maclean, D. J.; Cammue, B. P.; Ebert, P. R.; Manners, J. M. Pathogen-responsive expression of a putative ATP-binding cassette transporter gene conferring resistance to the diterpenoid sclareol is regulated by multiple defense signaling pathways in *Arabidopsis*. *Plant physiology* **2003**, *133*, 1272−1284.
(30) Johnson, S. R.; Bhat, W. W.; Bibik, J.; Turmo, A.; Hamberger, B.; Hamberger, B.; Boachon, B.; Buell, C. R.; Crisovan, E.; Dudareva, N. A database-driven approach identifies additional diterpene synthase activities in the mint family (*Lamiaceae*). *J. Biol. Chem.* **2019**, *294*, 1349−1362.
(31) Miller, G. P.; Bhat, W. W.; Lanier, E. R.; Johnson, S. R.; Mathieu, D. T.; Hamberger, B. The biosynthesis of the anti-microbial diterpenoid leubethanol in *Leucophyllum frutescens* proceeds via an all-cis prenyl intermediate. *Plant Journal* **2020**, *104*, 693−705.
(32) Hamberger, B.; Ohnishi, T.; Hamberger, B.; Séguin, A.; Bohlmann, J. Evolution of diterpene metabolism: Sitka spruce CYP720B4 catalyzes multiple oxidations in resin acid biosynthesis of conifer defense against insects. *Plant physiology* **2011**, *157*, 1677−1695.
(33) Vermaas, J. V.; Bentley, G. J.; Beckham, G. T.; Crowley, M. F. Membrane permeability of terpenoids explored with molecular simulation. *J. Phys. Chem. B* **2018**, *122*, 10349−10361.
(34) Vanommeslaeghe, K.; MacKerell, A. D., Jr Automation of the CHARMM General Force Field (CGenFF) I: bond perception and atom typing. *J. Chem. Inf. Model.* **2012**, *52*, 3144−3154.
(35) Vanommeslaeghe, K.; Hatcher, E.; Acharya, C.; Kundu, S.; Zhong, S.; Shim, J.; Darian, E.; Guvench, O.; Lopes, P.; Vorobyov, I.; et al. CHARMM general force field: A force field for drug-like molecules compatible with the CHARMM all-atom additive biological force fields. *Journal of computational chemistry* **2010**, *31*, 671−690.
(36) Vanommeslaeghe, K.; Raman, E. P.; MacKerell, A. D., Jr Automation of the CHARMM General Force Field (CGenFF) II: assignment of bonded parameters and partial atomic charges. *J. Chem. Inf. Model.* **2012**, *52*, 3155−3168.
(37) Kim, S.; Chen, J.; Cheng, T.; Gindulyte, A.; He, J.; He, S.; Li, Q.; Shoemaker, B. A.; Thiessen, P. A.; Yu, B.; et al. PubChem in 2021: new data content and improved web interfaces. *Nucleic acids research* **2021**, *49*, D1388−D1395.
(38) Kumar, A.; Yoluk, O.; MacKerell, A. D., Jr FFParam: Standalone package for CHARMM additive and Drude polarizable force field parametrization of small molecules. *Journal of computational chemistry* **2020**, *41*, 958−970.
(39) Frisch, M. J.et al.*Gaussian ∼ 16*, Revision C.01; Gaussian Inc. Wallingford, CT, 2016.
(40) Besler, B. H.; Merz, K. M., Jr; Kollman, P. A. Atomic charges derived from semiempirical methods. *Journal of computational chemistry* **1990**, *11*, 431−439.
(41) Singh, U. C.; Kollman, P. A. An approach to computing electrostatic charges for molecules. *Journal of computational chemistry* **1984**, *5*, 129−145.
(42) Brooks, B. R.; Brooks, C. L., III; Mackerell, A. D., Jr; Nilsson, L.; Petrella, R. J.; Roux, B.; Won, Y.; Archontis, G.; Bartels, C.; Boresch, S.; et al. CHARMM: the biomolecular simulation program. *Journal of computational chemistry* **2009**, *30*, 1545−1614.
(43) Vanommeslaeghe, K.; Yang, M.; MacKerell, A. D., Jr Robustness in the fitting of molecular mechanics parameters. *Journal of computational chemistry* **2015**, *36*, 1083−1101.
(44) Daum, G.; Tuller, G.; Nemec, T.; Hrastnik, C.; Balliano, G.; Cattel, L.; Milla, P.; Rocco, F.; Conzelmann, A.; Vionnet, C.; et al. Systematic analysis of yeast strains with possible defects in lipid metabolism. *Yeast* **1999**, *15*, 601−614.
(45) Lindberg, L.; Santos, A. X.; Riezman, H.; Olsson, L.; Bettiga, M. Lipidomic profiling of *Saccharomyces cerevisiae* and *Zygosaccharomyces bailii* reveals critical changes in lipid composition in response to acetic acid stress. *PloS one* **2013**, *8*, No. e73936.
(46) Ejsing, C. S.; Sampaio, J. L.; Surendranath, V.; Duchoslav, E.; Ekroos, K.; Klemm, R. W.; Simons, K.; Shevchenko, A. Global analysis of the yeast lipidome by quantitative shotgun mass spectrometry. *Proc. Natl. Acad. Sci. U. S. A.* **2009**, *106*, 2136−2141.
(47) Fei, Q.; O'Brien, M.; Nelson, R.; Chen, X.; Lowell, A.; Dowe, N. Enhanced lipid production by *Rhodosporidium toruloides* using different fed-batch feeding strategies with lignocellulosic hydrolysate as the sole carbon source. *Biotechnology for biofuels* **2016**, *9*, 1−12.
(48) Laursen, T.; Borch, J.; Knudsen, C.; Bavishi, K.; Torta, F.; Martens, H. J.; Silvestro, D.; Hatzakis, N. S.; Wenk, M. R.; Dafforn, T. R.; et al. Characterization of a dynamic metabolon producing the defense compound dhurrin in sorghum. *Science* **2016**, *354*, 890−893.
(49) Lorent, J.; Levental, K.; Ganesan, L.; Rivera-Longsworth, G.; Sezgin, E.; Doktorova, M.; Lyman, E.; Levental, I. Plasma membranes are asymmetric in lipid unsaturation, packing and protein shape. *Nat. Chem. Biol.* **2020**, *16*, 644−652.

(50) Jo, S.; Kim, T.; Iyer, V. G.; Im, W. CHARMM-GUI: a web-based graphical user interface for CHARMM. *Journal of computational chemistry* **2008**, *29*, 1859−1865.
(51) Kohlmeyer, A.; Vermaas, J.*TopoTools* (2017), DOI: 10.5281/zenodo.545655
(52) Humphrey, W.; Dalke, A.; Schulten, K. VMD: visual molecular dynamics. *J. Mol. Graphics* **1996**, *14*, 33−38.
(53) Kawakami, T.; Tahara, M.; Ikarashi, Y. Rosin-Related Compounds (Abietic Acid Derivatives) Concentrations in Chloroprene Rubber Products and the Amounts Eluted Into Artificial Sweat. *Dermatitis* **2022**, *33*, e47−e48.
(54) Walter, A.; Gutknecht, J. Monocarboxylic acid permeation through lipid bilayer membranes. *J. Membr. Biol.* **1984**, *77*, 255−264.
(55) Lee, C. T.; Comer, J.; Herndon, C.; Leung, N.; Pavlova, A.; Swift, R. V.; Tung, C.; Rowley, C. N.; Amaro, R. E.; Chipot, C.; et al. Simulation-based approaches for determining membrane permeability of small compounds. *J. Chem. Inf. Model.* **2016**, *56*, 721−733.
(56) Vermaas, J. V.; Crowley, M. F.; Beckham, G. T. Molecular simulation of lignin-related aromatic compound permeation through gram-negative bacterial outer membranes. *J. Biol. Chem.* **2022**, *298*, 102627.
(57) Lee, S.; Tran, A.; Allsopp, M.; Lim, J. B.; Hénin, J.; Klauda, J. B. CHARMM36 united atom chain model for lipids and surfactants. *J. Phys. Chem. B* **2014**, *118*, 547−556.
(58) Jorgensen, W. L.; Chandrasekhar, J.; Madura, J. D.; Impey, R. W.; Klein, M. L. Comparison of simple potential functions for simulating liquid water. *J. Chem. Phys.* **1983**, *79*, 926−935.
(59) Phillips, J. C.; Hardy, D. J.; Maia, J. D.; Stone, J. E.; Ribeiro, J. V.; Bernardi, R. C.; Buch, R.; Fiorin, G.; Hénin, J.; Jiang, W.; et al. Scalable molecular dynamics on CPU and GPU architectures with NAMD. *J. Chem. Phys.* **2020**, *153*, 044130.
(60) Feller, S. E.; Zhang, Y.; Pastor, R. W.; Brooks, B. R. Constant pressure molecular dynamics simulation: the Langevin piston method. *J. Chem. Phys.* **1995**, *103*, 4613−4621.
(61) Miyamoto, S.; Kollman, P. A. Settle: An analytical version of the SHAKE and RATTLE algorithm for rigid water models. *Journal of computational chemistry* **1992**, *13*, 952−962.
(62) Essmann, U.; Perera, L.; Berkowitz, M. L.; Darden, T.; Lee, H.; Pedersen, L. G. A smooth particle mesh Ewald method. *J. Chem. Phys.* **1995**, *103*, 8577−8593.
(63) Darden, T.; York, D.; Pedersen, L. Particle mesh Ewald: An N log (N) method for Ewald sums in large systems. *J. Chem. Phys.* **1993**, *98*, 10089−10092.
(64) Fletcher, R.*Numerical analysis*; Springer: 1976; pp 73−89.
(65) Van Der Walt, S.; Colbert, S. C.; Varoquaux, G. The NumPy array: a structure for efficient numerical computation. *Computing in science & engineering* **2011**, *13*, 22−30.
(66) Hunter, J. D. Matplotlib: A 2D graphics environment. *Computing in science & engineering* **2007**, *9*, 90−95.
(67) Sheinerman, F. B.; Brooks, C. L. Molecular picture of folding of a small α/β protein. *Proc. Natl. Acad. Sci. U. S. A.* **1998**, *95*, 1562−1567.
(68) Vermaas, J. V.; Petridis, L.; Qi, X.; Schulz, R.; Lindner, B.; Smith, J. C. Mechanism of lignin inhibition of enzymatic biomass deconstruction. *Biotechnology for biofuels* **2015**, *8*, 1−16.
(69) Vermaas, J. V.; Tajkhorshid, E. Differential membrane binding mechanics of synaptotagmin isoforms observed in atomic detail. *Biochemistry* **2017**, *56*, 281−293.
(70) Vermaas, J. V.; Rempe, S. B.; Tajkhorshid, E. Electrostatic lock in the transport cycle of the multidrug resistance transporter EmrE. *Proc. Natl. Acad. Sci. U. S. A.* **2018**, *115*, E7502−E7511.
(71) Zheng, F.; Vermaas, J. V.; Zheng, J.; Wang, Y.; Tu, T.; Wang, X.; Xie, X.; Yao, B.; Beckham, G. T.; Luo, H. Activity and thermostability of GH5 endoglucanase chimeras from mesophilic and thermophilic parents. *Applied and environmental microbiology* **2019**, *85*, e02079.
(72) Venable, R. M.; Krämer, A.; Pastor, R. W. Molecular dynamics simulations of membrane permeability. *Chem. Rev.* **2019**, *119*, 5954−5997.
(73) Diamond, J. M.; Katz, Y. Interpretation of nonelectrolyte partition coefficients between dimyristoyl lecithin and water. *J. Membr. Biol.* **1974**, *17*, 121−154.
(74) Bennion, B. J.; Be, N. A.; McNerney, M. W.; Lao, V.; Carlson, E. M.; Valdez, C. A.; Malfatti, M. A.; Enright, H. A.; Nguyen, T. H.; Lightstone, F. C.; et al. Predicting a drug's membrane permeability: A computational model validated with in vitro permeability assay data. *J. Phys. Chem. B* **2017**, *121*, 5228−5237.
(75) Marrink, S. J.; Berendsen, H. J. Permeation process of small molecules across lipid membranes studied by molecular dynamics simulations. *J. Phys. Chem.* **1996**, *100*, 16729−16738.
(76) Sugita, Y.; Kitao, A.; Okamoto, Y. Multidimensional replica-exchange method for free-energy calculations. *J. Chem. Phys.* **2000**, *113*, 6042−6051.
(77) Fiorin, G.; Klein, M. L.; Hénin, J. Using collective variables to drive molecular dynamics simulations. *Mol. Phys.* **2013**, *111*, 3345−3362.
(78) Sindhikara, D. J.; Emerson, D. J.; Roitberg, A. E. Exchange often and properly in replica exchange molecular dynamics. *J. Chem. Theory Comput.* **2010**, *6*, 2804−2808.
(79) Ferguson, A. L. BayesWHAM: A Bayesian approach for free energy estimation, reweighting, and uncertainty quantification in the weighted histogram analysis method. *J. Comput. Chem.* **2017**, *38*, 1583−1605.
(80) Habeck, M. Bayesian estimation of free energies from equilibrium simulations. *Phys. Rev. Lett.* **2012**, *109*, 100601.
(81) Hummer, G. Position-dependent diffusion coefficients and free energies from Bayesian analysis of equilibrium and replica molecular dynamics simulations. *New J. Phys.* **2005**, *7*, 34.
(82) Gaalswyk, K.; Awoonor-Williams, E.; Rowley, C. N. Generalized Langevin methods for calculating transmembrane diffusivity. *J. Chem. Theory Comput.* **2016**, *12*, 5609−5619.
(83) Fujimoto, K.; Nagai, T.; Yamaguchi, T. Momentum removal to obtain the position-dependent diffusion constant in constrained molecular dynamics simulation. *J. Comput. Chem.* **2021**, *42*, 2136−2144.
(84) Bonomi, M.; Camilloni, C. Biomolecular Simulations. *Methods Mol. Biol.* **2019**, *2022*, 2022.
(85) Matsson, P.; Doak, B. C.; Over, B.; Kihlberg, J. Cell permeability beyond the rule of 5. *Advanced drug delivery reviews* **2016**, *101*, 42−61.
(86) Seo, S.; Seto, H.; Koshino, H.; Yoshida, S.; Ohashi, Y. A diterpene as an endogenous signal for the activation of defense responses to infection with tobacco mosaic virus and wounding in tobacco. *Plant Cell* **2003**, *15*, 863−873.
(87) Sharma, E.; Anand, G.; Kapoor, R. Terpenoids in plant and arbuscular mycorrhiza-reinforced defence against herbivorous insects. *Annals of Botany* **2017**, *119*, 791−801.
(88) McGarvey, D. J.; Croteau, R. Terpenoid metabolism. *plant cell* **1995**, *7*, 1015.
(89) Souza, A. B.; de Souza, M. G.; Moreira, M. A.; Moreira, M. R.; Furtado, N. A.; Martins, C. H.; Bastos, J. K.; Dos Santos, R. A.; Heleno, V. C.; Ambrosio, S. R.; et al. Antimicrobial evaluation of diterpenes from *Copaifera langsdorffii* oleoresin against periodontal anaerobic bacteria. *Molecules* **2011**, *16*, 9611−9619.
(90) Molina-Salinas, G. M.; Rivas-Galindo, V. M.; Said-Fernández, S.; Lankin, D. C.; Munoz, M. A.; Joseph-Nathan, P.; Pauli, G. F.; Waksman, N. Stereochemical analysis of leubethanol, an anti-TB-active serrulatane, from *Leucophyllum frutescens*. *J. Nat. Prod.* **2011**, *74*, 1842−1850.
(91) Gonzalez, M. A.; Correa-Royero, J.; Agudelo, L.; Mesa, A.; Betancur-Galvis, L. Synthesis and biological evaluation of abietic acid derivatives. *Eur. J. Med. Chem.* **2009**, *44*, 2468−2472.
(92) Raza, S.; Miller, M.; Hamberger, B.; Vermaas, J. V.*Plant Terpenoid Permeability through Biological Membranes Explored via Molecular Simulations*. 2022; DOI: 10.5281/zenodo.7183240.
(93) Towns, J.; Cockerill, T.; Dahan, M.; Foster, I.; Gaither, K.; Grimshaw, A.; Hazlewood, V.; Lathrop, S.; Lifka, D.; Peterson, G. D.;

Roskies, R.; Scott, J. R.; Wilkins-Diehr, N. XSEDE: Accelerating Scientific Discovery. *Comput. Sci. Eng.* **2014**, *16*, 62−74.

https://doi.org/10.1021/acs.jpcb.2c07209
J. Phys. Chem. B 2023, 127, 1144−1157